ELSEVIER

Volume 183, Issue 2, February 2010

JOURNAL OF SOLID STATE CHEMISTRY

www.elsevier.com/locate/jssc

CONTENTS

Abstracted/indexed in BioEngineering Abstracts, Chemical Abstracts, Coal Abstracts, Current Contents/Physics, Chemical, & Earth Sciences, Engineering Index, Research Alert, SCISEARCH, Science Abstracts, and Science Citation Index. Also covered in the abstract and citation database SCOPUS®. Full text available on ScienceDirect®.

Regular Articles

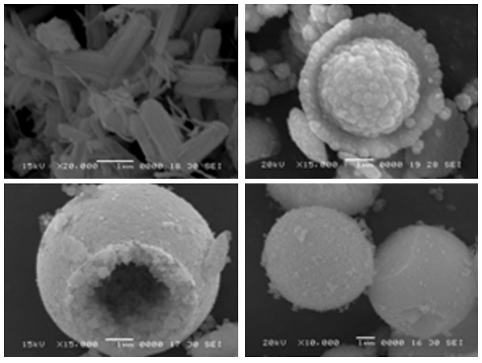

Mesoporous Co_3O_4 and CeO_2 with different morphologies, such as micrometer-sized rod, hollow sphere, saucer-like sphere, and solid sphere were synthesized by nanocasting.

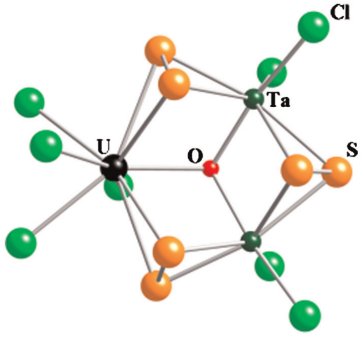

The UTa2O(S2)3Cl6 cluster with completed coordination sphere around uranium.

Regular Articles—Continued

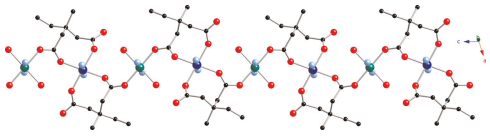

Five two-dimensional divalent cobalt coordination polymers containing 4,4′-bipyridine (bpy) and substituted or unsubstituted glutarate ligands have been prepared and structurally characterized by single-crystal X-ray diffraction. Three contain dimeric $\{Co_2(CO_2)_2\}$ units, while two manifest $\{Co(CO_2)\}_n$ chains, depending on the steric bulk of the substituent. The magnetic properties of the complexes were analyzed successfully with a recently developed phenomenological chain model accounting for both magnetic coupling (J) and zero-field splitting effects (D).

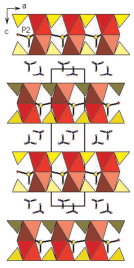

The 2-D structure of $(NH_4)_2Co_2(HPO_3)_3$ comprises anionic complex sheets with ammonium cations present between them. An anionic complex sheet contains three-deck phosphite units, which are interconnected by dimmeric Co_2O_9 to form complex layers.

Continued

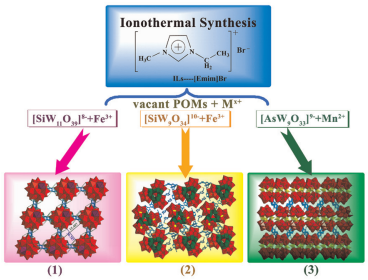

Three new transition-metal-containing polyoxotungstate hybrids were synthesized successfully under the ionothermal condition, which proves that the ionothermal synthesis is a suitable synthetic method for different kinds of polyoxometalates.

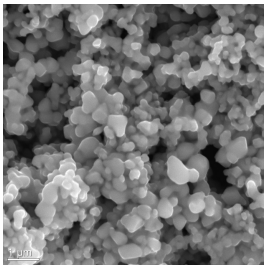

The disordered, β-phase of lithium ferrite is sustained by air quenching from 900 °C. Shown is a SEM image of β-$LiFe_5O_8$ exhibiting even particle sizes less than 300 nm.

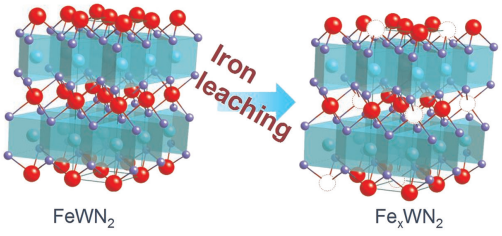

Non-stoichiometric Fe_xWN_2 ($x \sim 0.72$) was synthesized via leaching of Fe from layer-structured stoichiometric $FeWN_2$ by soaking in sulfuric acid at ca. 50 °C.

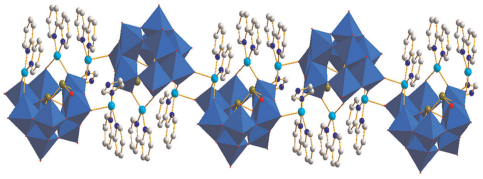

We report the synthesis, crystal structure and electrochemical and magnetic properties of the new lacunary arsenotungstate substituted simultaneously arsenide fragment and copper complexes.

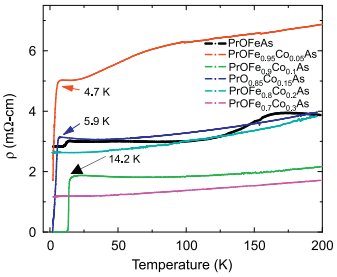

Cobalt doping at the iron site in PrOFeAs (semimetal) compound suppresses structural distortion and spin density wave with the evolution of superconductivity. The Seebeck and Hall coefficient (R_H) indicate electron type charge carriers in these compounds and charge carrier density increases with increase in Co-doping. Temperature dependence of resistivity (ρ) for (a) PrOFeAs, (b) $PrOFe_{0.95}Co_{0.05}As$, (c) $PrOFe_{0.9}Co_{0.1}As$, (d) $PrOFe_{0.85}Co_{0.15}As$, (e) $PrOFe_{0.8}Co_{0.2}As$ and (f) $PrOFe_{0.7}Co_{0.3}As$.

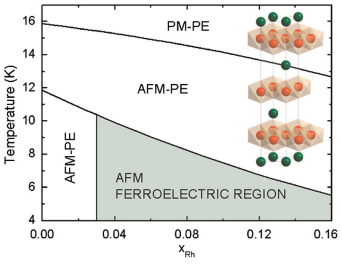

Polycrystalline samples of the delafossite solid solution $CuFe_{1-x}Rh_xO_2$ were synthesized and characterized. Polarization has been observed in the range $0.02 < x \le 0.15$ with characteristic temperatures in coincidence with magnetic transition temperatures.

Magnetic relaxation behavior of lanthanide substituted Dawson-type tungstoarsenates

Lizhen Liu, Fengyan Li, Lin Xu, Xizheng Liu and Guanggang Gao

Page 350

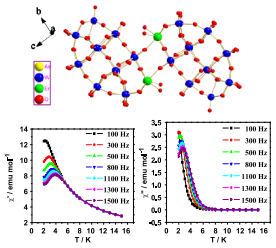

Two polyoxometalate compounds $[(CH_3)_4N]_8[Ln(H_2O)_8]_2[(\alpha_2\text{-}As_2W_{17}O_{61})Ln(H_2O)_2]_2 \cdot nH_2O$ (Ln = Er (**1**), Dy (**2**)) have been prepared. The dynamic magnetic measurements for **2** display a slow relaxation of magnetization, showing a frequency-dependent susceptibility.

Solvothermal indium fluoride chemistry: Syntheses and crystal structures of $K_5In_3F_{14}$, β-$(NH_4)_3InF_6$ and $[NH_4]_3[C_6H_{21}N_4]_2[In_4F_{21}]$

Anil C.A. Jayasundera, Richard J. Goff, Yang Li, Adrian A. Finch and Philip Lightfoot

Page 356

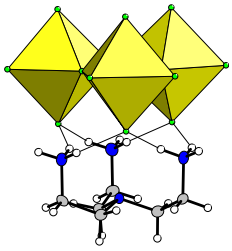

Solvothermal synthesis has been used to prepare three indium fluorides, including a novel hybrid material containing a unique $[In_3F_{15}]$ trimer templated by *tren*.

Synthesis, crystal structure, and photocatalytic activity of the new three-layer aurivillius phases, $Bi_2ASrTi_2TaO_{12}$ (A = Bi, La)

Dong Wang, Kaibin Tang, Zhenhua Liang and Huagui Zheng

Page 361

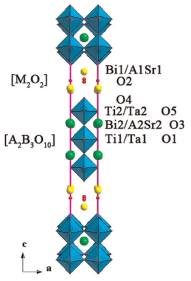

Two new three-layer Aurivillius phases $Bi_2ASrTi_2TaO_{12}$ (A = Bi, La) have been synthesized by a conventional solid state reaction method. And this is the crystal structure of the three-layer Aurivillius phases, $Bi_2ASrTi_2TaO_{12}$.

Hydrogenation of palladium rich compounds of aluminium, gallium and indium

H. Kohlmann

Page 367

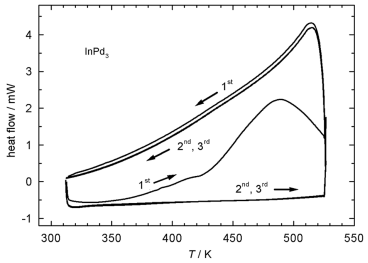

In situ differential scanning calorimetry of the hydrogenation of tetragonal $InPd_3$ ($ZrAl_3$ type) at 1.3 MPa hydrogen pressure.

A high temperature superionic phase of $CsSn_2F_5$

P. Berastegui, S. Hull and S.G. Eriksson

Page 373

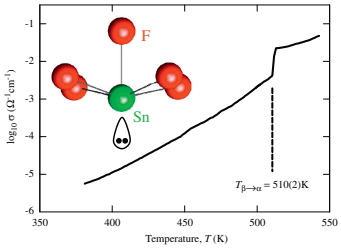

$CsSn_2F_5$ is shown to undergo a first order phase transition at 510(2) K to a superionic phase in which the specific electronic configuration of the Sn^{2+} plays a key role in promoting extensive disorder of the anions.

Structural refinement of $T_2Mo_3O_8$ (T = Mg, Co, Zn and Mn) and anomalous valence of trinuclear molybdenum clusters in $Mn_2Mo_3O_8$

Hideki Abe, Akira Sato, Naohito Tsujii, Takao Furubayashi and Masahiko Shimoda

Page 379

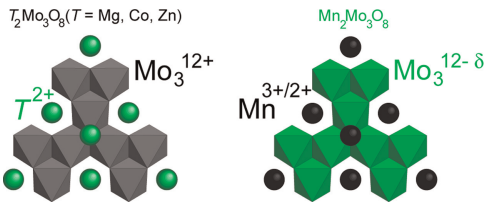

Trinuclear Mo_3 clusters in $Mn_2Mo_3O_8$ adopt an anomalous valence of $12-\cong$ ($\cong > 0$) unlike the Mo_3^{12+} clusters that are usually recognized for Mo_3-containing inorganic compounds including $T_2Mo_3O_8$ (T = Mg, Co or Zn).

Continued

Fabrication and electron transport properties of epitaxial films of electron-doped $12CaO \cdot 7Al_2O_3$ and $12SrO \cdot 7Al_2O_3$
Masashi Miyakawa, Hidenori Hiramatsu, Toshio Kamiya, Masahiro Hirano and Hideo Hosono
Page 385

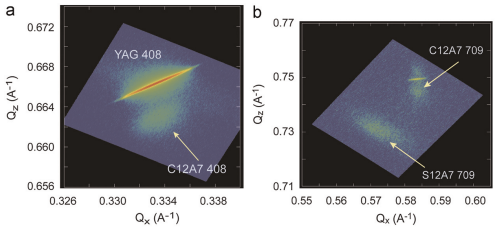

Reciprocal space maps around the 408 and the 709 diffractions show the films were grown epitaxially with the orientation relationship of (001)[100] $12SrO \cdot 7Al_2O_3$ || (001)[100] $12CaO \cdot 7Al_2O_3$ || (001)[100] $Y_3Al_5O_{12}$.

Neutron diffraction study of the crystal structure and structural phase transition of $La_{0.7}Ca_{0.3-x}Sr_xCrO_3$ ($0 \le x \le 0.3$) The relationship between thermodynamic behavior and crystal structure changes at the phase transition
Kazuki Omoto, Stefan T. Norberg, Steve Hull, Akimitsu Aoto and Takuya Hashimoto
Page 392

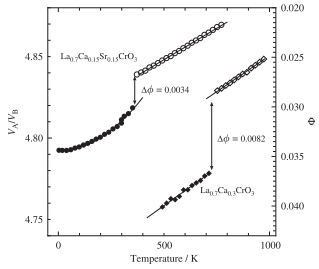

Temperature dependence of parameter, Φ, representing the extent of distortion from the ideal cubic perovskite structure, for $La_{0.7}Ca_{0.3}CrO_3$ (diamonds) and $La_{0.7}Ca_{0.15}Sr_{0.15}CrO_3$ (circles) calculated from neutron diffraction patterns.

High-pressure crystal growth and magnetic and electrical properties of the quasi-one dimensional osmium oxide Na_2OsO_4
Y.G. Shi, Y.F. Guo, S. Yu, M. Arai, A.A. Belik, A. Sato, K. Yamaura, E. Takayama-Muromachi, T. Varga and J.F. Mitchell
Page 402

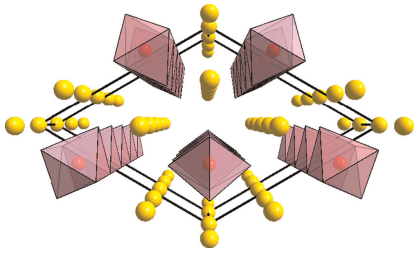

Na_2OsO_4 crystals were grown by a NaCl flux method under high pressure. It crystallizes in the Ca_2IrO_4-type structure comprising infinite $Os^{6+}O_6$ octahedra ($5d^2$) chains. The crystal growth, the crystal structure, and the magnetic and electrical properties are reported.

$LiZnNb_4O_{11.5}$: A novel oxygen deficient compound in the Nb-rich part of the Li_2O–ZnO–Nb_2O_5 system
Vladimir A. Morozov, Alla V. Arakcheeva, Vera V. Konovalova, Philip Pattison, Gervais Chapuis, Oleg I. Lebedev, Valery V. Fomichev and Gustaaf Van Tendeloo
Page 408

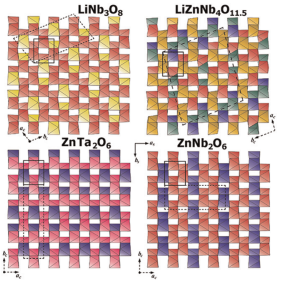

$LiZnNb_4O_{11.5}$ with an original α-PbO_2 related structure has been found in the Nb-rich part of Li_2O–ZnO–Nb_2O_5 system and characterized by X-ray diffraction and transition electron microscopy (TEM). Using synchrotron powder diffraction data, the structure has been solved and refined by means of both commensurate modulation and supercell models.

On the symmetry and crystal structures of Ba_2LaIrO_6
W.T. Fu, R.J. Götz and D.J.W. IJdo
Page 419

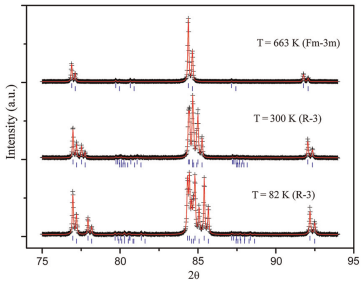

Observed (crosses) and calculated (continuous line) profiles of Ba_2LaIrO_6 at some selected temperature showing the region containing the basic (222), (321) and (400) reflections. Tick marks below indicate the positions of the allowed Bragg's reflections.

Cooperative effect of monoclinic distortion and sinusoidal modulation in the martensitic structure of Ni_2FeGa
J.B. Lu, H.X. Yang, H.F. Tian, L.J. Zeng, C. Ma, L. Feng, G.H. Wu, J.Q. Li and J. Jansen
Page 425

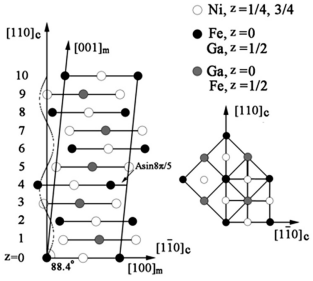

The structural model of the "5M" Ni_2FeGa martensite viewed along the $[001]_c$ (i.e. $[010]_m$) zone axis, demonstrating the cooperative effect of monoclinic distortion and sinusoidal modulation along the $[110]_c$ direction.

$NaAlF_4$: Preparation, crystal structure and thermal stability
Sergei D. Kirik and Julia N. Zaitseva
Page 431

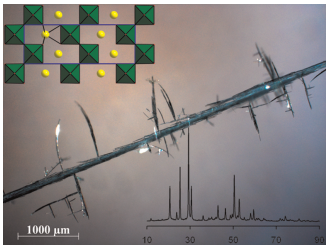

The compound $NaAlF_4$ was for the first time described 55 years ago, but until now it was not properly studied. Meantime the phase is responsible for the most low-melting part of the $NaF–AlF_3$ system, which is the great importance for the aluminum production. The lack of information about $NaAlF_4$ is due to narrow interval of stability which is close to liquid part of the system.

Structural, electronic and optical properties of orthorhombic $CdGeO_3$ from first principles calculations
C.A. Barboza, J.M. Henriques, E.L. Albuquerque, E.W.S. Caetano, V.N. Freire and J.A.P. da Costa
Page 437

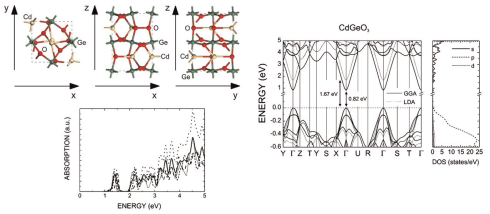

Different views of the unit cell of orthorhombic $CdGeO_3$ (left, top). The electronic band structure near the main gap and the partial density of states (PDOS) are shown also (right), as well as the optical absorption for different polarizations of incident light (left, bottom).

Synthesis, structure and theoretical studies of a new ternary non-centrosymmetric β-$LaGaS_3$
Peng Li, Long-Hua Li, Ling Chen and Li-Ming Wu
Page 444

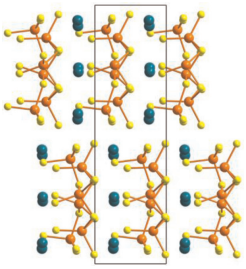

New non-centrosymmeteic ternary lanthanum gallium sulfide, β-$LaGaS_3$, features the wavy GaS_4 tetrahedron chains that are separated by La^{3+} cations has been synthesized by a solid state reaction. Such an orthorhombic β-$LaGaS_3$ is isomeric with the monoclinic α-$LaGaS_3$. Detailed structural differences between the title compound and its isomer, monoclinic α-$LaGaS_3$, are discussed. The absorption spectra and electronic structures of both types of $LaGaS_3$ have been calculated with the aid of WIEN2k package as well as the refractive indexes, absorption coefficients and reflectivities. The calculated band gap and absorption edge of β-$LaGaS_3$ agree well with the experimental measurements. And a weak NLO response of β-$LaGaS_3$ has been detected.

Homogeneous one-dimensional structured $Tb(OH)_3$:Eu^{3+} nanorods: Hydrothermal synthesis, energy transfer, and tunable luminescence properties
Jun Yang, Guogang Li, Chong Peng, Chunxia Li, Cuimiao Zhang, Yong Fan, Zhenhe Xu, Ziyong Cheng and Jun Lin
Page 451

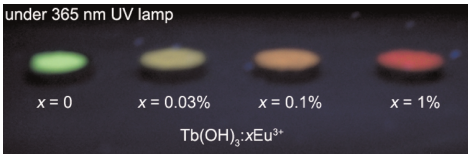

The colors of $Tb(OH)_3$:xEu^{3+} phosphors can be easily tuned from green, yellow, orange, to red due to different energy transfer occurs from Tb^{3+} to Eu^{3+}.

Crystal growth, crystal structure of new polymorphic modification, β-$Bi_2B_8O_{15}$ and thermal expansion of α-$Bi_2B_8O_{15}$
R.S. Bubnova, J.V. Alexandrova, S.V. Krivovichev, S.K. Filatov and A.V. Egorysheva
Page 458

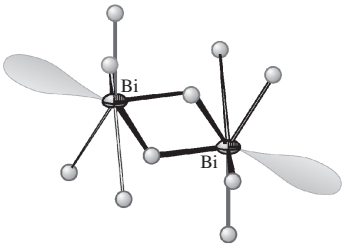

Typical Bi_2O_2 unit in crystal structure of α- and β-$Bi_2B_8O_{15}$.

Crystal growth, structure and magnetic properties of the double perovskites Ln_2MgIrO_6 (Ln = Pr, Nd, Sm–Gd)
Samuel J. Mugavero III, Adam H. Fox, Mark D. Smith and Hans-Conrad zur Loye
Page 465

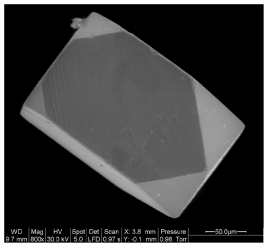

A SEM image of a typical crystal of Ln_2MgIrO_6, which forms in the monoclinic double perovskite structure, is shown.

Continued

$Gd_4B_4O_{11}F_2$: Synthesis and crystal structure of a rare-earth fluoride borate exhibiting a new "fundamental building block" in borate chemistry

Almut Haberer, Reinhard Kaindl and Hubert Huppertz

Page 471

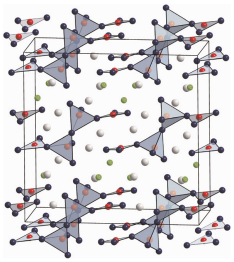

A new gadolinium fluoride borate $Gd_4B_4O_{11}F_2$ could be synthesized via high-pressure/high-temperature synthesis (multianvil technique). The crystal structure exhibits a structural motif not yet reported from borate chemistry: two BO_4-tetrahedra (□) and two BO_3-groups (Δ) are connected via common corners, leading to the fundamental building block 2Δ2□:Δ□□Δ.

A novel nanocomposite material prepared by intercalating photoresponsive dendrimers into a layered double hydroxide

Toshiyuki Tanaka, Shunsuke Nishimoto, Yoshikazu Kameshima, Junpei Matsukawa, Yasuhiko Fujita, Yutaka Takaguchi, Motohide Matsuda and Michihiro Miyake

Page 479

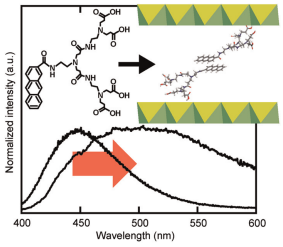

A novel inorganic–organic nanocomposite material, a layered double hydroxide (LDH) containing photoresponsive dendrimers in the interlayer space, was successfully prepared through an ion-exchange reaction. The resulting material exhibited unique photochemical properties, compared to those of the bare photoresponsive dendrimer molecule.

Rapid Communication

Multiband orange–red photoluminescence of Eu^{3+} ions in new "114" $LnBaZn_3GaO_7$ and $LnBaZn_3AlO_7$ oxides

M.P. Saradhi, B. Raveau, V. Caignaert and U.V. Varadaraju

Page 485

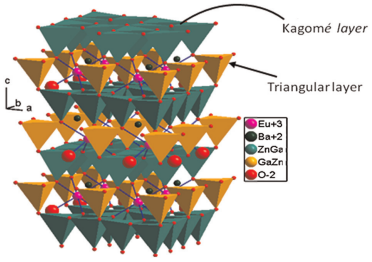

The projected structure consists of alternate stacked layers of Kagomé and Triangular type with statistical distribution of Zn and Ga atoms between two tetrahedral sites. Ba^{2+} present in anticuboctahedron coordinating with 12 oxygen atoms. The Eu^{3+} present in octahedral coordination with 3-fold rotational symmetry.